Magnetization reversal in cobalt antidot arrays

L. J. Heyderman,* F. Nolting, D. Backes,† and S. Czekaj
Paul Scherrer Institut, 5232 Villigen-PSI, Switzerland

L. Lopez-Diaz
Departamento Fisica Aplicada, Universidad de Salamanca, Pza. de la Merced, Salamanca 37008, Spain

M. Kläui and U. Rüdiger
Fachbereich Physik, Universität Konstanz, Universitätsstrasse 10, Konstanz, Germany

C. A. F. Vaz and J. A. C. Bland
Cavendish Laboratory, University of Cambridge, Madingley Road, Cambridge, CB3 0HE, United Kingdom

R. J. Matelon‡ and U. G. Volkmann
Facultad de Física, Pontificia Universidad Católica de Chile, Santiago, Chile

P. Fischer
LBNL/CXRO, 1 Cyclotron Road, Berkeley, California 94720, USA

We have carried out a detailed study of the magnetic switching in square lattice cobalt antidot arrays with periods ranging from 2 μm down to 200 nm (antidot size=antidot separation). Magneto-optical Kerr effect measurements show first a small change in the magnetization due to a reversible rotation of the magnetic spins in the antidot rows, followed by a large change due to reversal of the antidot array columns parallel to the applied field. Employing x-ray photoemission electron microscopy and transmission x-ray microscopy, the latter irreversible process was observed as a nucleation and propagation of discrete domain chains. The propagating chain ends are blocked by perpendicular chains present in the antidot rows via various mechanisms revealed by micromagnetic simulations.

I. INTRODUCTION

Patterned magnetic thin films[1] are of significant interest due to the novel magnetic effects at reduced lateral dimensions and also because of their potential for industrial applications such as high density information storage and sensor devices.[2–5] While small isolated magnetic elements have been very much the focus of scientific endeavor, another fascinating class of patterned magnetic films comprising a continuous film containing a regular array of nonmagnetic inclusions or holes, referred to as antidot arrays, is receiving increased attention. Antidot arrays are particularly of interest because, as a result of the stray field energy associated with the holes, their introduction into a continuous magnetic thin film or multilayer system will significantly modify the magnetic properties resulting in novel domain configurations, additional magnetic anisotropies, and modification of the magnetization reversal, which in turn affects the switching fields and magnetoresistance behavior.[6–11] By choosing a specific antidot geometry, with a given antidot size, antidot separation, and lattice symmetry and orientation, it is therefore possible to control the magnetic properties. The dynamic behavior of antidot arrays is also attracting much interest because the spin wave spectra is dramatically different to that of continuous magnetic thin films,[12–15] with localized modes occurring in specific regions confined by the holes within the antidot lattice.

The basic domain configuration for square antidot arrays with the antidot size ≥ the antidot separation is given in Fig. 1, observed as a periodic checked domain contrast commensurate with the antidot lattice with photoemission electron microscopy (PEEM).[16,17] Similar configurations were seen with magnetic force microscopy (MFM)[6,8,11] and transmission electron microscopy,[18] and correlate well with micromagnetic simulations.[19,20] The switching field increases as the antidot period decreases[7,8] and this was attributed to the increased pinning of the domain walls in the vicinity of the antidots, although very little is known about the details of the switching processes.

A study using MFM on square antidot arrays with antidot size and separation of 1.6 and 1.4 μm, indicated that the arrays switch in columns parallel to the applied field.[6] However, the measurements were limited to an area of 8 × 8 μm^2, and gave no information about the exact nature of the switching. Our recent observation of chains of magnetic domains, having discrete lengths corresponding to multiples of the antidot period,[16,17] gave some indication of the magnetic spin configuration during the reversal process. In order to determine exactly how the magnetization reversal progresses, we have carried out a detailed study of the switching behavior of cobalt antidot arrays on application of an in-plane magnetic field, and report here the details of the domain chain nucleation, propagation, and pinning. The observations were carried out on antidot arrays with periods ranging from 2 μm down to 200 nm and with antidot size =antidot separation using photoemission electron microscopy (PEEM) and transmission x-ray microscopy (TXM).
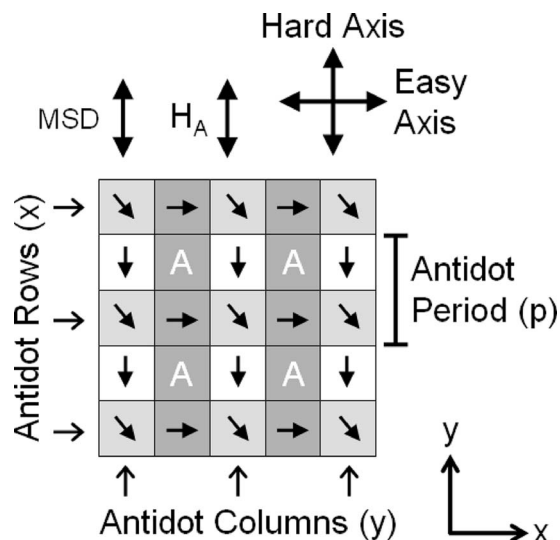
FIG. 1. Schematic diagram of the antidot geometry with the position of the square antidots marked with the letter A. The expected XMCD contrast is included for a magnetization sensitivity direction (MSD) along y. The antidot columns are parallel to y and the rows are parallel to x. The easy and hard axes are along the x and y directions, respectively, and the field is applied parallel (or at a small angle) to y.

Comparing the observations with micromagnetic simulations and magneto-optical Kerr effect (MOKE) measurements, we were able to identify the key mechanisms behind the observed reversal behavior.

We find that when the field is applied almost parallel to the antidot array columns, which we define as the y direction (see Fig. 1), reversal not only occurs via the growth of domain chains along y but also by the growth of perpendicular domain chains along x. The observed increase of the switching field with decreasing period can be explained by an increase in the energy barriers associated with nucleation and depinning of domain chains. The location of the ends of the y domain chains is modified by the presence of the perpendicular domain chains during reversal; orthogonal chain ends coincide to form a stable domain wall configuration and propagating chains are blocked as they approach perpendicular chains by the formation of a 360° wall, often resulting in the occurrence of chain ends in the same row. The annihilation of such 360° walls provides an additional energy barrier, observed as small domains remaining towards the end of magnetization reversal.

II. EXPERIMENTAL DETAILS

Electron beam lithography was employed to fabricate the antidot arrays. In a first step, the antidot pattern was written with a Leica LION LV1 electron beam writer in a polymethylmethacrylate resist (PMMA) on a silicon (001) substrate. The pattern was then transferred into polycrystalline cobalt films with a thickness $t=10$ nm, capped with a 1-nm-thick aluminum layer to prevent oxidation, and deposited by dc-magnetron sputtering (base pressure $=2 \times 10^{-6}$ mbar). The pattern transfer involved a lift-off pro-

cess to give a cobalt film with periodic arrays of holes. In addition, 40-nm-thick cobalt films were deposited onto prepatterned silicon substrates containing arrays of holes with a depth of 140 nm. To fabricate the prepatterned substrate, the antidot pattern in the PMMA resist was first transferred using reactive ion etching (RIE) into a chromium thin film, which was subsequently used as a mask to etch holes into the silicon by RIE.[21] The latter process was developed for fabrication of antidot arrays on silicon nitride membranes required for TXM (the details of which we plan to publish later), with a thicker cobalt film to enhance the magnetic contrast. While the detailed studies presented here were mainly carried out on the 10-nm-thick films, it should be noted that for the 40-nm-thick films deposited on prepatterned substrates, there may be a small influence on the domain configuration due to stray field coupling between the continuous cobalt film with an array of holes and the corresponding cobalt dot array deposited in the lower etched regions.

We have concentrated our study on antidot arrays with the antidot size equal to the antidot separation, where the stray field energy associated with the antidots is sufficient to give a checked domain configuration (see representation of XMCD contrast in Fig. 1) and chains of magnetic domains have been observed.[16,17] The periods, p, range from 2 μm down to 200 nm. Due to the limited resolution of the fabrication process, as the period decreases, the antidots change in geometry from square to round holes at around $p=300$ nm. While this change in shape will have an effect on the detailed magnetic spin configurations, we expect that the general behavior of the domain chains will not differ significantly. The antidot arrays cover a square area with side length of 10–20 μm, and in order to obtain a large enough area for MOKE measurements, several of the 20×20 μm^2 arrays were assembled close together with a 2 μm separation. The cobalt film has a small uniaxial anisotropy and the antidot arrays were fabricated with the intrinsic easy and hard axes of the cobalt film oriented approximately parallel to the array rows (along x) and columns (along y), respectively (see schematic of geometry in Fig. 1).

The imaging of the magnetic domains was carried out at the SIM beamline[22] at the Swiss Light Source, Paul Scherrer Institut, with an Elmitec PEEM.[23] Employing x-ray magnetic circular dichroism (XMCD), the magnetic domains were imaged by tuning the x-ray energy to the Co L_3-edge. Dividing two images taken with left and right circular polarized light leads to an image with increased magnetic contrast which we refer to as an XMCD image. Here the intensity is a measure of the angle between the circular x-ray polarization vector, labeled as the magnetization sensitivity direction (MSD) in the figures, and the magnetic spins in the domains.[24] Ferromagnetic domains with magnetic spins parallel or antiparallel to the polarization vector (or MSD) appear black or white in the XMCD image, while domains with magnetic spins perpendicular to the polarization vector will have a gray contrast. A two-dimensional map of the magnetization can be determined from two XMCD images of the same area with orthogonal magnetization sensitivity directions, obtained by rotating the sample by 90° about the surface normal. For observations of the magnetization reversal, the samples were mounted in a magnetizing holder which allowed the *in situ*
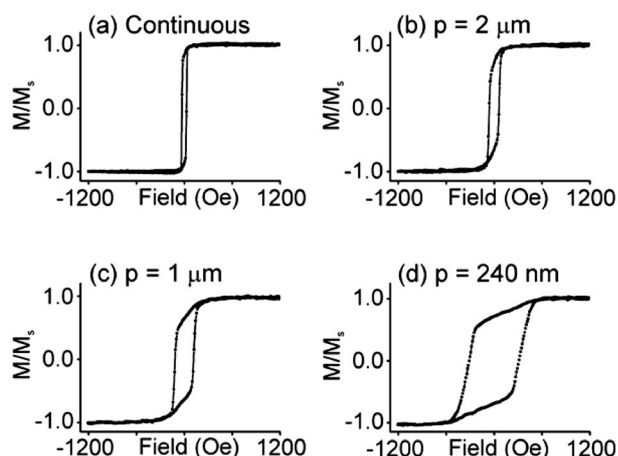
FIG. 2. Hysteresis loops obtained from longitudinal MOKE measurements, with the field applied parallel to y: (a) for a 10–nm-thick continuous film and (b)-(d) for antidot arrays $t=10$ nm which show an increase in switching field as the antidot period, p, decreases. The initial small change in the magnetization corresponds to rotation of the magnetic spins in the antidot rows and the large change to the reversal of the antidot columns.

application of in-plane magnetic fields up to 300 Oe. The field was always applied parallel (or almost parallel) to the antidot array columns along y (see schematic of geometry in Fig. 1), and the direction of the applied field is indicated by an arrow and labeled H_A in the figures. Pulsed currents could be applied to the magnetizing holder to provide much larger fields which, although not calibrated, helped to saturate the sample. It is difficult to obtain an XMCD image in an applied field which disturbs the low energy electrons in the PEEM. Therefore we restricted our PEEM observations to the remanent states, i.e., after reducing the applied field to zero. Complementary TXM observations were carried out in applied fields using magnetic transmission soft x-ray microscopy[25] at the XM-1 beamline at the Advanced Light Source in Berkeley.

III. MAGNETIZATION REVERSAL

The hysteresis loops obtained from longitudinal MOKE measurements for antidot arrays with different periods (t $=10$ nm) and with the field applied parallel to the antidot array columns (y), are given in Fig. 2. For comparison, the hysteresis loops of a 100 μm square cobalt film without antidots (referred to as a continuous film) were also measured. The continuous film displayed a uniaxial anisotropy, with the easy and hard axes oriented close to x and y, respectively. The anisotropy field value is about 15 Oe and the easy axis coercivity is about 20 Oe. For all of the antidot arrays, the hysteresis loops measured for fields applied along x and y are virtually identical indicating the dominance of the antidots in the reversal behavior over the intrinsic anisotropy of the cobalt film. All of the antidot array hysteresis loops [Figs. 2(b)–2(d)] are characterized by two main features. First there is a small decrease in the magnetization after saturation which corresponds to a rotation of the magnetic spins in the
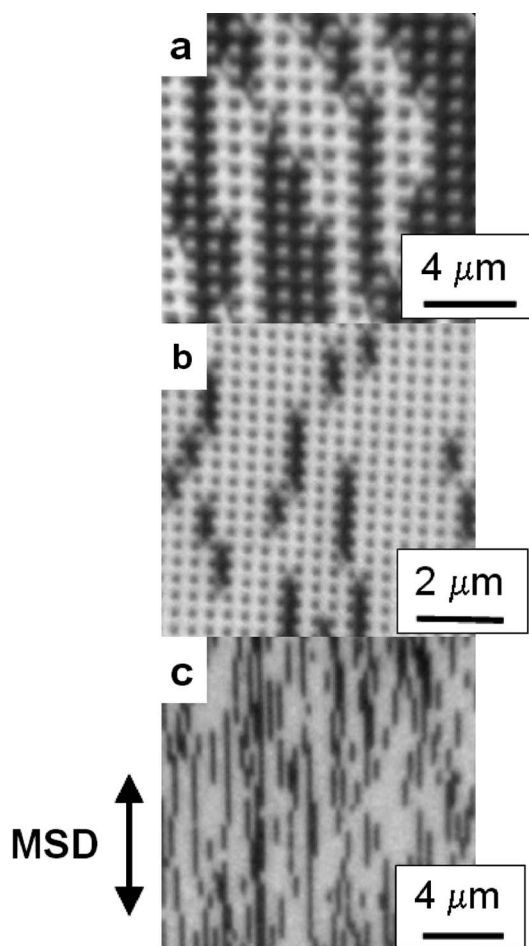

FIG. 3. XMCD images taken with PEEM of domain chains in 10-nm-thick antidot arrays with $p=$ (a) 1 μm, (b) 400 nm, and (c) 240 nm.

antidot rows to give the basic antidot configuration in Fig. 1. Here the magnetic spins neighboring the antidots rotate to align themselves parallel to the antidot borders in order to reduce the stray field energy and at the intersections the magnetic spins rotate to 45°. The second feature of the hysteresis loops is a subsequent large change in the magnetization corresponding to the switching of the antidot columns (along y) in the field direction. In addition, as the antidot period decreases there is an increase in switching field as reported in Refs. 7, 8, and 11, and an increase in the field range in which the first reversible process occurs.

The reversal of the antidot columns in the second part of the hysteresis loops occurs via nucleation and propagation of domain chains and was observed for all antidot array periods studied here (ranging between 200 nm and 2 μm, with antidot size=antidot separation). Examples of the domain chains in antidot arrays with different antidot periods (all with $t=10$ nm) are given in Fig. 3 and the full magnetization reversal process for the $p=1$ μm antidot array is shown in Fig. 4. Here the magnetic field is applied parallel to the antidot columns, along y, and the magnetization sensitivity direction is also along y, so that the XMCD contrast is sensitive to reversal occurring in the columns. With the aim of saturating the antidot array along the field direction, first a
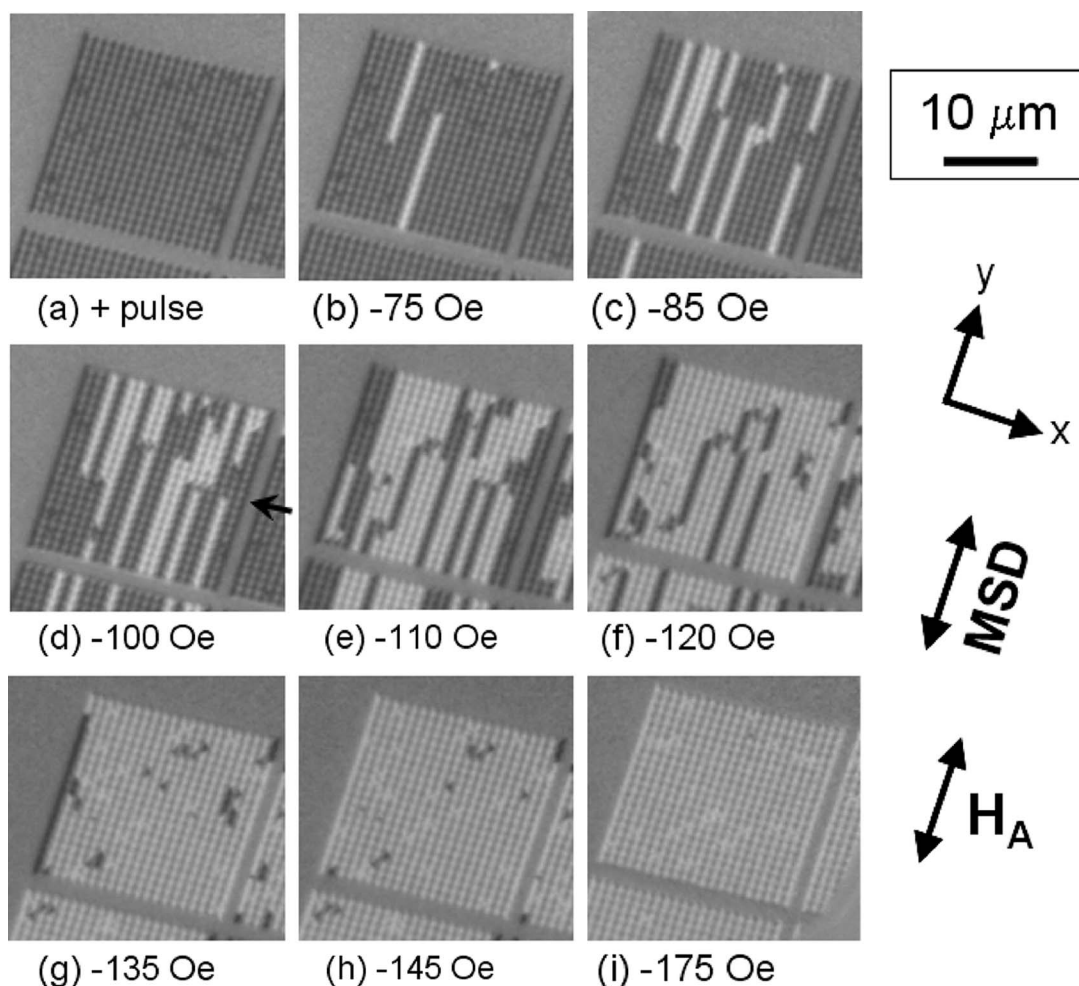
FIG. 4. Magnetization reversal via domain chains observed with PEEM in a 10-nm-thick antidot array with $p=1$ μm. The array is first saturated with a positive field pulse >195 Oe, and the resulting remanent states are given after decreasing the field to zero (a) and applying increasing negative fields (b) to (i).

positive field pulse >195 Oe was applied and a high remanence magnetic state was observed after reducing the field down to 0 Oe [Fig. 4(a)]. The field was then increased to a small value in the reverse direction, and subsequently reduced to zero in order to observe the remanent state. This was repeated several times, observing the development of the remanent states after applying a negative field with gradually increasing values. It can be seen in Fig. 4 that once nucleated, the domain chains propagate to a particular length where the ends are pinned, while new domain chains nucleate in other parts of the array. The majority of the switching via chain nucleation and propagation occurs between -85 and -110 Oe [Figs. 4(c)–4(e)], while small domain chains, with lengths of only a few antidot periods, remain up to -145 Oe [Figs. 4(g) and 4(h)] until the array saturates [Fig. 4(i)]. In order to measure the magnetic contrast sensitive to the perpendicular spin orientation during magnetization reversal, the sample holder was rotated by 90° about the surface normal (Fig. 5). Here it becomes apparent that the antidot rows also switch via nucleation and propagation of chains of domains, this time perpendicular to those in Fig. 4 and at a higher field range above -135 Oe [Fig. 5(c)]. The

reversal in the antidot rows indicates that the field was not applied perfectly parallel (at a degree or so) to the antidot array columns.

To further elucidate the reversal processes, micromagnetic simulations were performed using the OOMMF package (http://math.nist.gov/oommf/) on a 10-nm-thick cobalt film containing a square lattice antidot array with area 1.9 $\times 1.9$ μm^2 and square antidots with $p=200$ nm (corresponding to the smallest period of the samples), and using a simulation cell size of 5×5 nm^2. Typical parameters for cobalt were chosen; magnetization at saturation, $M_S=1400$ $\times 10^3$ A/m, exchange constant, $A=3\times10^{-11}$ J/m, and uniaxial anisotropy constant, $k_U=3.5\times10^3$ J/m^3. When the simulations were performed with the applied field exactly parallel to the array columns (along y), the domain chain configuration in the x direction remained virtually static with magnetic spins in each direction ($+x$ and $-x$) having equal probability. In order to better represent the reversal observed experimentally, with a switching of the rows along x, it was necessary to introduce a small offset angle (5°) to the applied field with respect to y. First, a positive field of 500 Oe was applied and then reduced to zero. The field was then in-
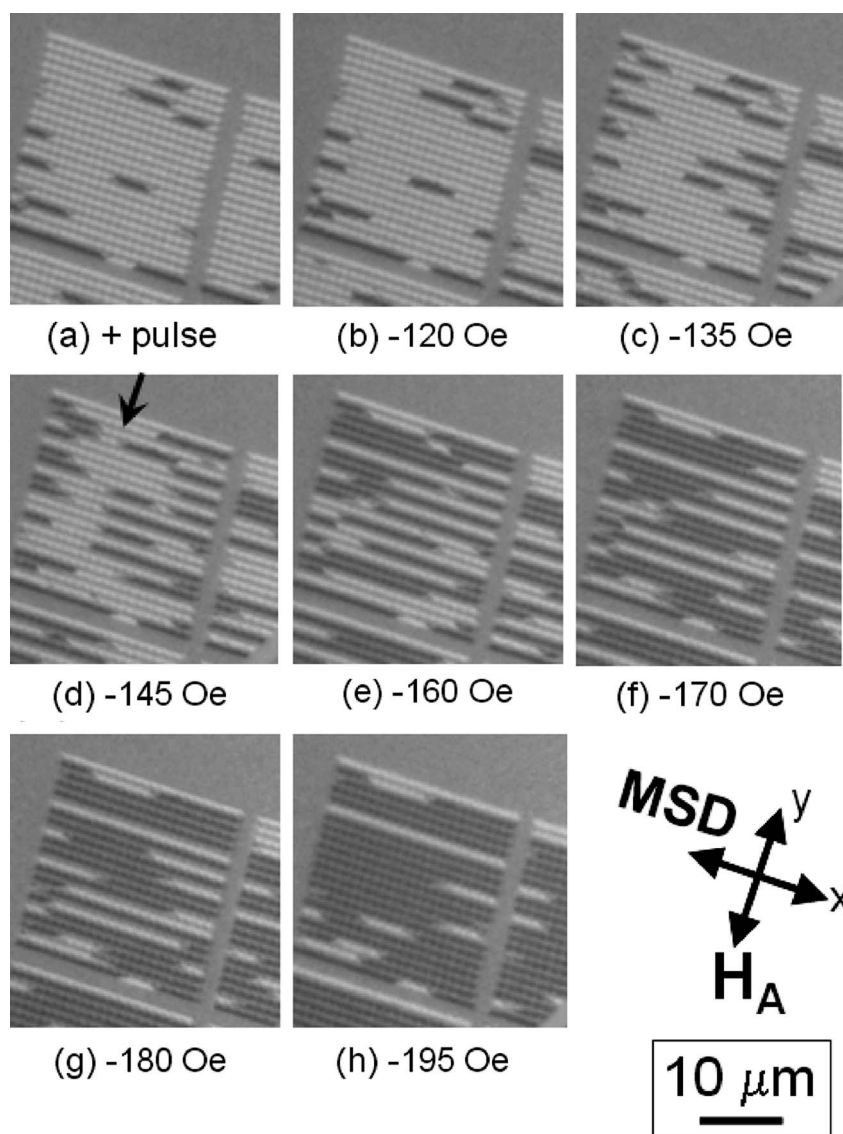
FIG. 5. Magnetization reversal in the antidot array in Fig. 4 ($t=10$ nm and $p=1$ μm), with the magnetic field applied in the same direction as in Fig. 4 but this time with the magnetization sensitivity direction rotated by 90°. Here we observe a reversal of the rows perpendicular to the applied field direction via domain chains along x.

creased in the negative sense in 50 Oe steps and, as in the PEEM measurements, the remanent states after reducing the field to zero were captured following each increase in field (Fig. 6). Similar to the experimental observations, at lower fields reversal takes place via domain chains along y and at higher fields, the rows (along x) also reverse via domain chains.

It can be seen in Fig. 6 that the ends of the domain chains forming in the columns (y) often coincide with the ends of the perpendicular domain chains along the rows (x), as indicated at several locations with round frames at $H_A=-550$ Oe. Indeed, by comparing pairs of XMCD images with orthogonal orientations of the magnetization sensitivity direction (MSD) in several antidot arrays of different periods, we observed many locations where the ends of two orthogonal domains coincide. An example is given in Fig. 7 for an antidot array with $t=40$ nm and $p=800$ nm where several coincident chain ends are indicated with round frames. On

closer inspection of the first remanent state of the simulation in Fig. 6 after applying a field of +500 Oe, small disturbances in the basic antidot configuration are visible as "magnetic defects" (indicated with arrows at $H_A=+500$ Oe), and correspond to the position of the ends of domain chains running along x. It seems likely that the black and white "spots" in the checked domain patterns of Figs. 4(a) and 4(i), respectively, are similar magnetic defects. Indeed, in the experiment it turns out that the positions of the magnetic defects, and therefore the ends of the x domain chains, often correspond to the position of the ends of the y domain chains which subsequently form.

IV. MAGNETIC SPIN CONFIGURATIONS

In order to better understand the mechanisms which govern reversal in the antidot arrays, we now take a closer look at the possible spin configurations present. Assuming the
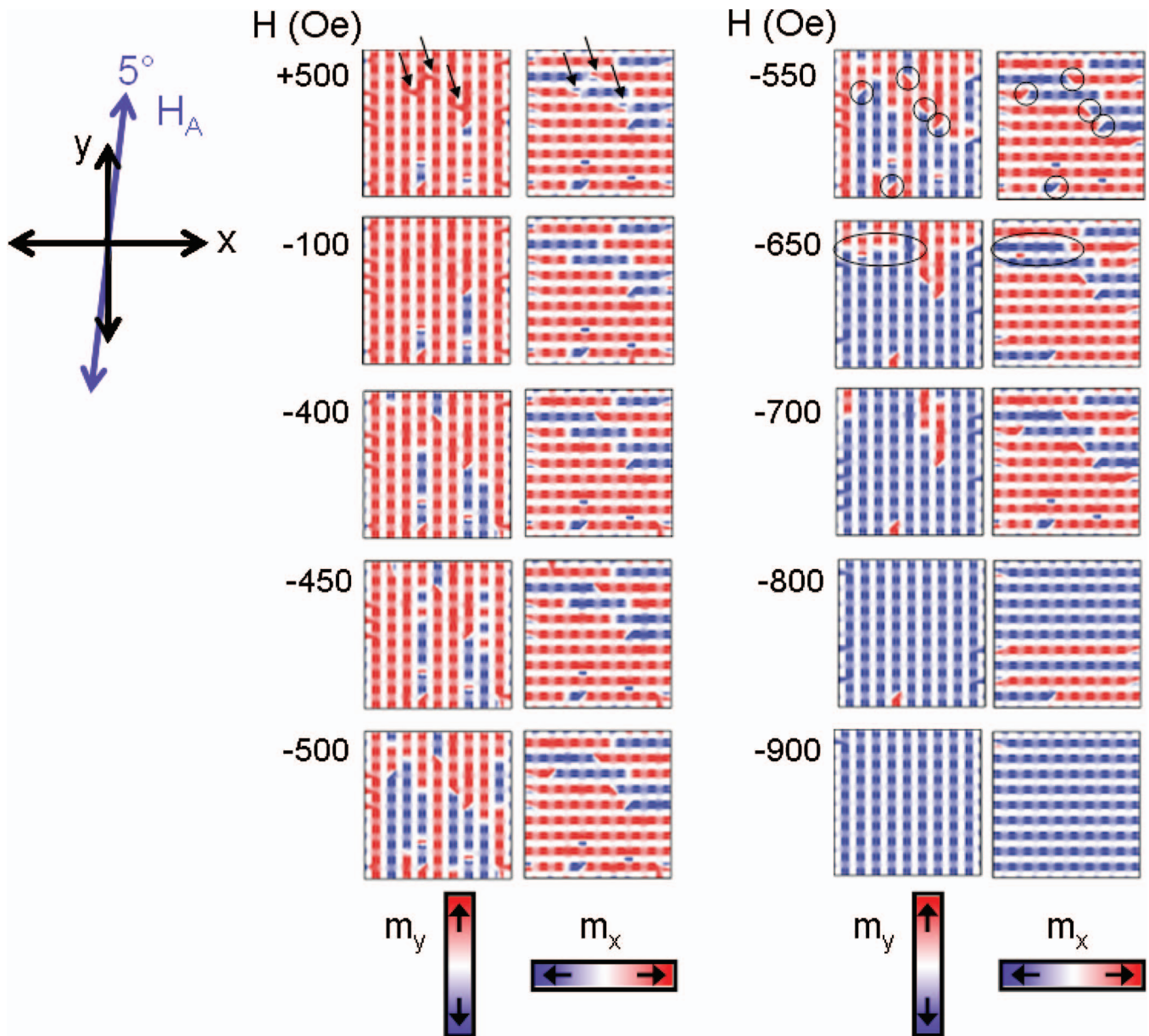
FIG. 6. (Color) Snapshots of a micromagnetic simulation of an antidot array with an area of 1.9×1.9 μm^2, with antidot size=antidot separation=100 nm, and a film thickness of 10 nm. First, a positive field of 500 Oe was applied and then reduced to zero. The field was then increased in the negative sense in 50 Oe steps and remanent states captured after each increase in field. The applied field is at a small angle (5°) to the hard axis resulting in a reversal of the rows along *x*. The arrows at $H_A=+500$ Oe indicate magnetic defects (magnetization sensitivity along *y*), which correspond to the ends of domain chains along *x*. The round frames at $H_A=-550$ Oe indicate locations where the ends of orthogonal chains coincide and the oval frames at $H_A=-650$ Oe indicate a row where several chain ends occur.

simple model that adjacent to the antidots the magnetic spins are parallel to the antidot borders and at the intersections the magnetic spins are at 45° as in Fig. 1, we would expect to see four different configurations of the magnetic spins surrounding the antidots as shown in Fig. 8(a): (A) circular, (B) cross, (C) C-state, and (D) leaf. We do indeed observe XMCD contrast which corresponds to these different states, as indicated in the two-dimensional map of the magnetization in an array with $p=1$ μm and $t=40$ nm in Fig. 8(b). However, looking at the details of the magnetic spins in the micromagnetic simulations [Fig. 8(c), $p=200$ nm], we see that in addition to the basic magnetic states, there is a more complex behavior

at the antidot intersections due to the formation of two types of domain wall at the chain ends: either 90° walls (vertical or horizontal) associated with diverging or converging magnetic spins [square frames in Fig. 8(c)] or 180° walls oriented at 45° [two walls enclosed by an oval frame in Fig. 8(c)]. The magnetic spin configurations at the intersections bounded between four antidots are schematically represented by diagrams E, F, and G. The basic antidot configuration with no domain wall present is configuration E. The configuration F occurs when two orthogonal chain ends coincide [indicated in the XMCD images of Figs. 7 and 8(b) by round frames], with two sets of opposing spins surrounding the intersection
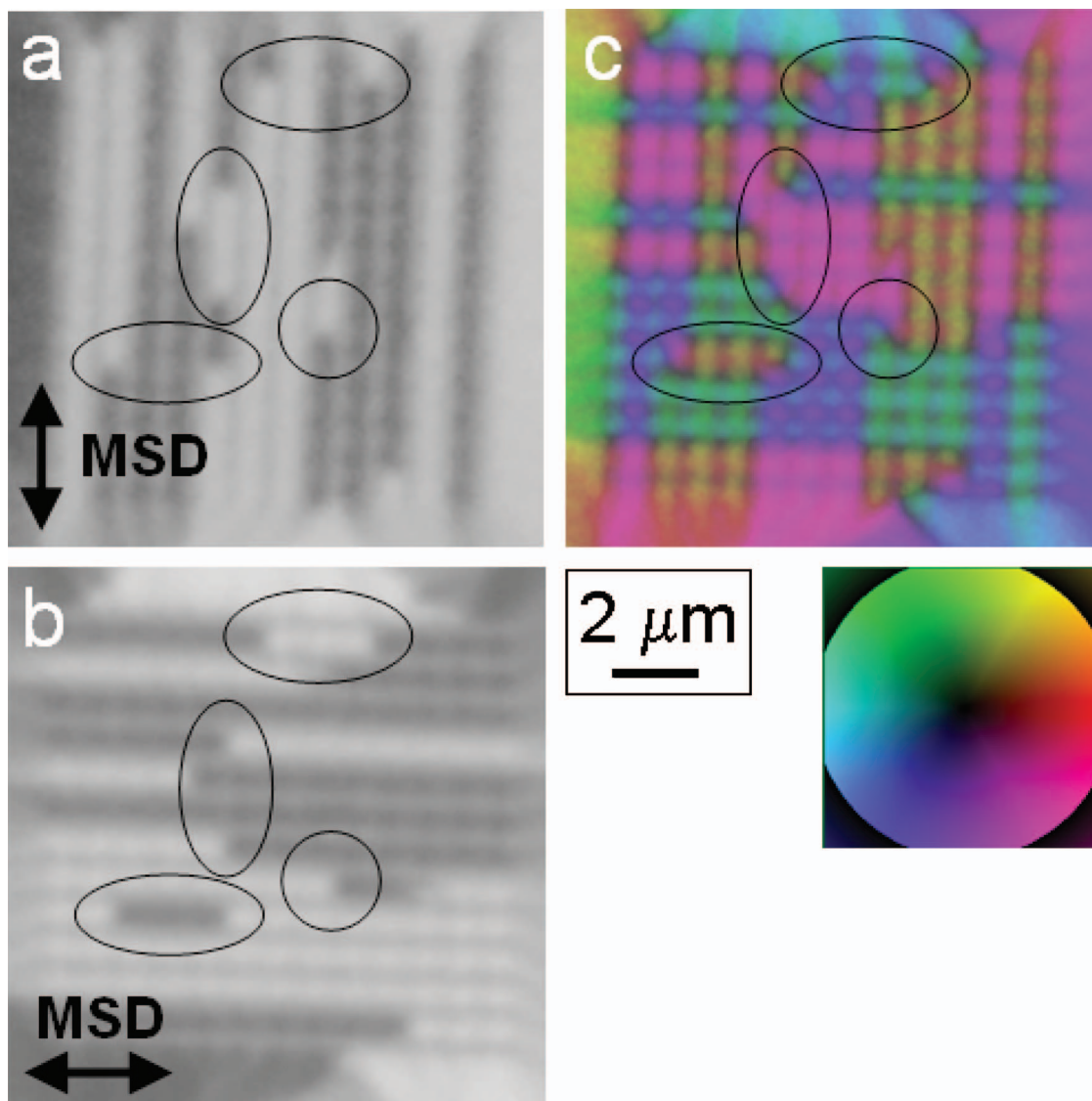
FIG. 7. (Color) XMCD images taken with PEEM of a 40-nm-thick antidot array with $p=800$ nm. (a) and (b) are the same array measured with orthogonal sensitivity directions, and (c) is the resulting two-dimensional color map determined from (a) and (b). The locations where the ends of orthogonal domains coincide are indicated with round frames.

resulting in a diagonal 180° wall and a low energy flux closure state. This results in a strong pinning of the propagating chain ends and also explains why the chain ends of orthogonal domains often coincide. Of course, for larger antidot separations, the resulting flux closure configurations can be more complex. Instances were observed experimentally where the ends of the domain chains do not coincide with the ends of orthogonal chains. In the simulation this corresponds to the second domain wall configuration, G, which occurs when there is only one set of opposing spins at the intersection leading to two 90° walls. This also results in a pinning of the domain walls although it is less favorable in terms of the stray field energy. There is one additional domain wall configuration at the ends of the domain chains which are present in the rows after application of a saturating field along y. This is an S-shape wall configuration and is seen, for example, in Fig. 6 after application of a field of +500 Oe (indicated by the arrows) and is schematically represented by

diagram H in Fig. 8(a). After application of a negative field, the S-walls transform into the 90° wall configuration I in Fig. 8(a) (equivalent to G but rotated by 90°), and eventually form the configuration F when two orthogonal chain ends coincide.

V. DETAILED REVERSAL MECHANISMS

By observing the detailed progression of the micromagnetic simulations to equilibrium after application or relaxation of the applied field, we can further understand the processes that govern the nucleation, propagation, and pinning of the domain chains. This is illustrated in Fig. 9, which comprises a series of snapshots of part of a simulation of an antidot array approaching equilibrium in an applied field. We see that domain nucleation occurs by formation of a diagonal domain, indicated at two locations with a round frame in Fig. 9. Domain propagation then occurs by expansion of the
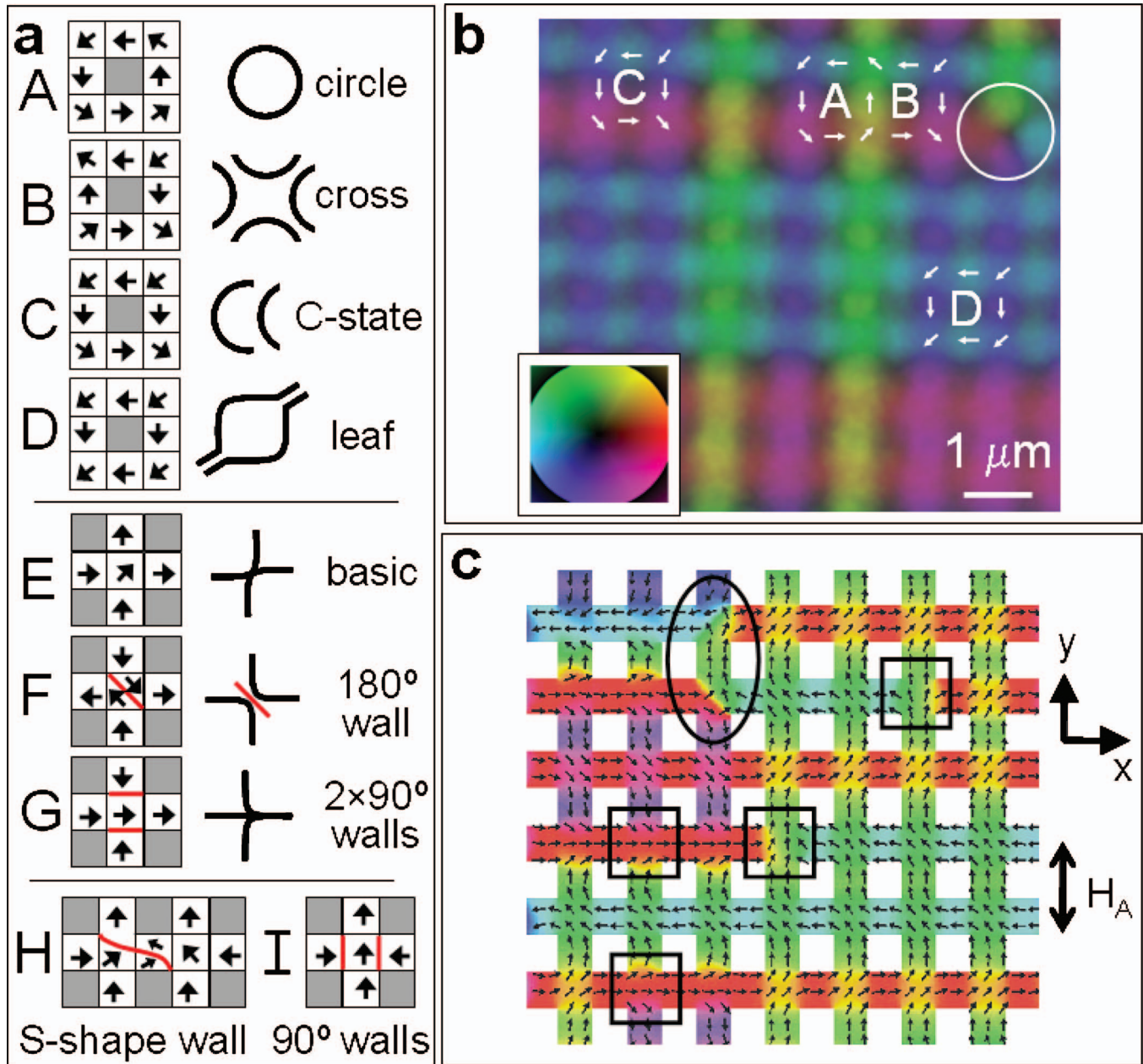
FIG. 8. (Color) (a) Schematic diagrams of the different antidot configurations surrounding an antidot (A to D), at the antidot intersection (E to G) and at the end of a perpendicular domain chain (H and I). (b) Two-dimensional XMCD image taken with PEEM of an antidot array with $p=1$ μm and $t=40$ nm, which includes contrast corresponding to the four basic configurations and a location where orthogonal chain ends coincide indicated by a round frame. (c) A color plot of a typical remanent state given by the micromagnetic simulations after application of a field of -450 Oe (field parallel to y, initial applied field: $+1000$ Oe) with four 90° walls indicated by square frames and two 180° walls indicated by an oval frame.

nucleated diagonal domains and advancement of the chain boundaries along the columns of the antidot array (y). The propagation of the domain chains along y can be blocked via three possible mechanisms: (i) intrinsic defects in the magnetic film (e.g., pores, surface roughness, and grain boundaries), (ii) extrinsic defects due to patterning (the antidots themselves and edge roughness created by the patterning), and (iii) the existing magnetic configuration, i.e., the presence of perpendicular chains in the antidot rows (along x). When no perpendicular chains are present during reversal, the first two effects will be responsible for pinning of the

propagating chain ends which, due to the presence of the antidots, are likely to give the 90° wall configuration G in Fig. 8(a). When perpendicular domains are present, there are two possible mechanisms responsible for restraining the propagating chain ends. The first is a pinning of the chain ends due to the formation of the flux closure 180° wall configuration F in Fig. 8(a) when orthogonal chain ends coincide. The second is a blocking of the chain ends propagating along y when they approach a perpendicular chain running along x, i.e., a row where the orientation of the spins along x reverses. Here a 360° wall forms, as indicated at several
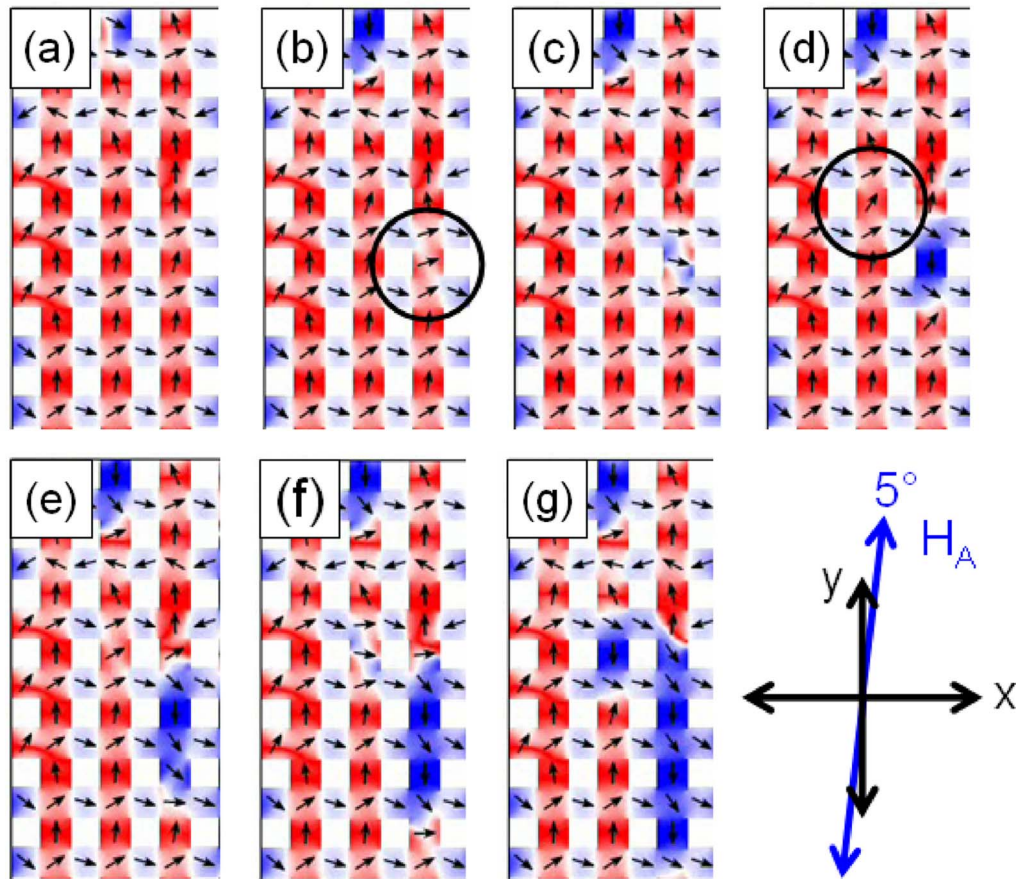
FIG. 9. (Color online) Details of the micromagnetic simulation shown in Fig. 6. Starting with the remanent state after an applied field of −450 Oe, these are snapshots of the development of the magnetic spins on application of negative field of −500 Oe. Nucleation occurs by formation of diagonal domains (round frames), followed by propagation of the chain ends along the antidot array columns.

locations by arrowheads in the simulation of the antidot array at equilibrium in an applied field in Fig. 10(a). The advancing chain ends are blocked due to the high exchange energy barrier associated with annihilation of 360° walls, also seen for 360° walls in continuous film systems[26] and small magnetic thin film elements.[5] On relaxation of the field, the chain ends relax back to the nearest pinning location forming either 90° or 180° walls, and often resulting in small domains [Fig. 10(b)] which were observed experimentally [Figs. 4(g) and 4(h)]. When several chain ends propagating along y approach the same perpendicular chain (a row in which the magnetic spin direction along x reverses), the blocking via formation of a 360° wall will result in the occurrence of several chain ends in the same row. In Fig. 10(a), several 360° walls form in the row indicated by the large arrow and on relaxation of the field, the chain ends recede to form a row of 90° walls indicated by the large arrow in Fig. 10(b). The alignment of chain ends in a row was not only observed in the micromagnetic simulations (see also region indicated by the oval frame in Fig. 6 at a field of −650 Oe) but also in the XMCD images [see rows indicated by arrows in Figs. 4(d) and 5(d)]. It should be noted that in the simulations several chains not only depin but also disappear on relaxation of the field [Figs. 10(a) and 10(b)]. Such behavior was not observed experimentally with TXM (not shown), where the applied field and remanent configurations were always found to be identical,

indicating a stronger pinning of the domain chain ends in real magnetic thin film antidot systems. As there was little difference between hysteretic and remanent experimental observations, we feel confident that the PEEM observations give a realistic insight into the magnetization reversal.

We have described above how the presence of perpendicular domain chains in the rows strongly influence the positions of the ends of chains forming in the columns during reversal in two ways: the ends of the perpendicular chain ends provide pinning centers and propagating domain chains can be blocked by perpendicular chains, resulting in the formation of chain ends in the same row. Indeed, we have seen in the simulations that when the applied field is sufficient to eliminate the perpendicular domain chains (i.e., under the same simulation conditions of Fig. 6, but starting with a positive field of 1000 Oe rather than 500 Oe), then the propagation of the chains is no longer blocked and the reversal along y occurs via a complete switching of the columns (of course, in real systems, intrinsic material defects or edge roughness of the antidots can serve as pinning sites in the absence of perpendicular domain chains). The perpendicular chains (along x) are likely to be present during reversal along y (close to the field direction) when the x-component of the applied field is not sufficient to remove them, and in particular when the applied field is exactly parallel to y. Small differences in the applied field strengths and orientation can
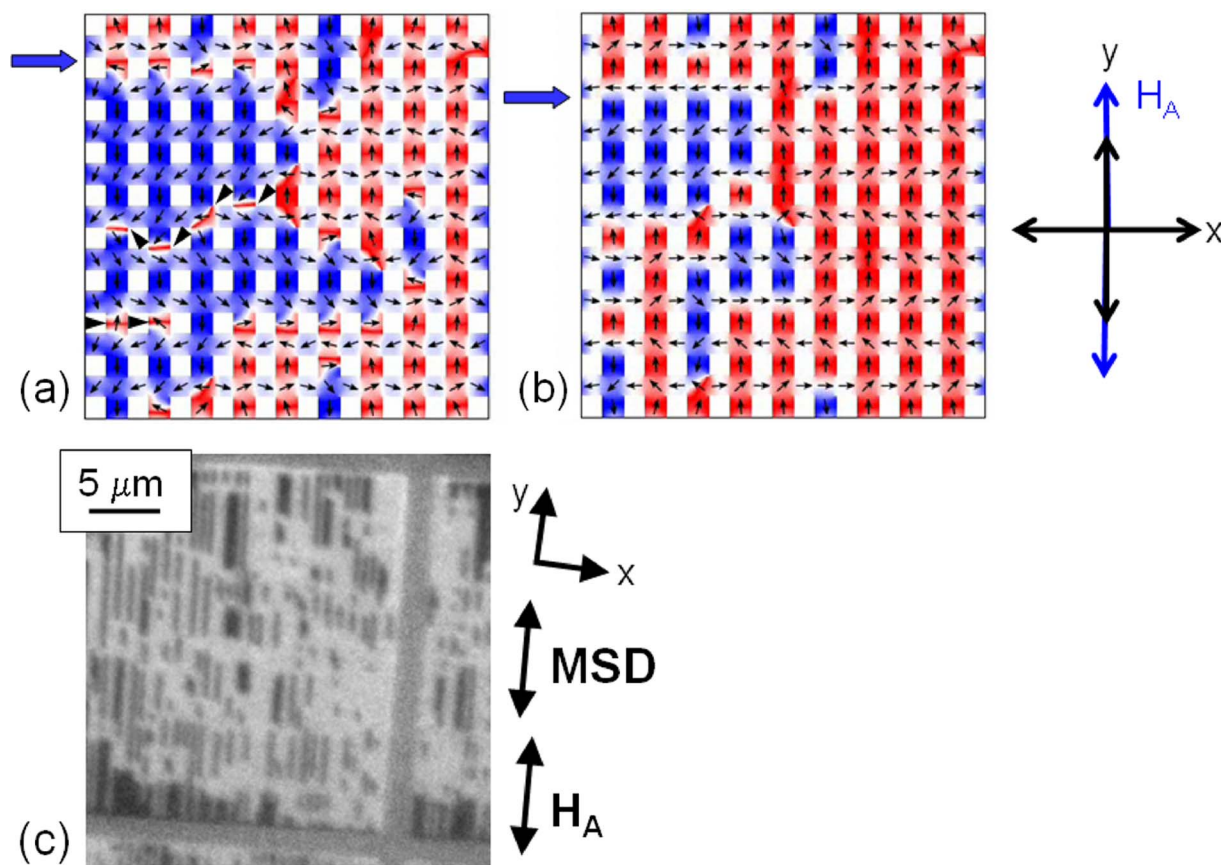
FIG. 10. (Color online) Details of a micromagnetic simulation similar to that shown in Fig. 6, but with the applied field parallel to y. Starting with the remanent state after an applied field of -450 Oe, (a) is the equilibrium state on application of a negative field of -500 Oe and (b) is the remanent state after subsequent relaxation of the field to zero. The black arrowheads in (a) indicate locations where $360°$ walls form as the propagating chain ends approach a perpendicular chain, i.e., where there is a reversal of the magnetic spin direction in the rows. Several propagating chain ends approach a perpendicular chain forming a row of $360°$ walls indicated by the large arrow in (a). After relaxation of the field, they form a row of $90°$ walls indicated by the large arrow in (b). (c) XMCD image taken with PEEM of domain chains in a 10-nm-thick antidot array with $p=240$ nm. The array was first saturated with a negative field of 280 Oe, and then the remanent states observed after application of increasing positive fields. This shows the remanent state after an applied field of 245 Oe and in contrast to Fig. 3(c), the domain chains form in bands indicating the presence of perpendicular domain chains during reversal.

therefore lead to very different reversal behavior. For example, the striking formation of domain chains in bands in the XMCD image of the $p=240$ nm antidot array in Fig. 10(c) indicates the presence of perpendicular domain chains during reversal. This domain configuration is very different to that in Fig. 3(c), where the virtually random positions of the chains imply that there are very few perpendicular chains present.

Finally, we address the question of what is responsible for the changes in the hysteresis loops observed on decreasing the antidot period, namely the increase in the switching field and the lengthening of the reversible region seen in Fig. 2. We have already seen that the pinning of the domain ends is important during magnetization reversal, i.e., the domain chains grow to a particular length where the chain ends are strongly pinned. This implies that the reversal of the columns, and therefore the switching field, is dominated by the energy barriers related to both domain nucleation and depinning of chain ends. When these barriers are overcome, the propagation of the chain boundaries occurs over several antidot periods until the next pinning center is reached, as

observed in the TXM on increasing the applied field in small steps (5–10 Oe). We can also infer from the simulations that an additional higher energy barrier is related to the annihilation of the $360°$ walls and results in small domains remaining towards the end of the reversal [Figs. 4(g) and 4(h)]. The exact height of these energy barriers is related to the extent of twisting of the magnetic spins (exchange energy contribution dominates) and collective rotation of magnetic spins (magnetostatic energy contribution is important) involved in a given reversal process. For example, for the annihilation of the $360°$ walls, it is the exchange energy contribution which mainly determines the height of the energy barrier. Both the exchange and magnetostatic contributions increase on reducing the antidot array period, i.e., decreasing the lateral dimensions, resulting in the observed increase in the switching field. The initial reversible part of the hysteresis loops involves a coherent rotation of the magnetic spins in the rows away from the field direction (along y) to give the basic antidot configuration in Fig. 1. As the antidot period decreases, this process starts earlier (at higher positive fields) because the higher stray field energy assists the alignment of

the spins with the antidot borders, and will end later (at higher negative fields) because the additional exchange energy at smaller lateral dimensions hinders the formation of the basic antidot configuration of Fig. 1.

VI. CONCLUSIONS

We have carried out a detailed study of the magnetization reversal in cobalt antidot arrays with periods ranging from 2 μm down to 200 nm and with applied fields parallel to the array columns. The switching occurs first by a reversible rotation of the magnetic spins identified as a small change in the magnetization in the MOKE hysteresis loops, and is followed by nucleation and propagation of domain chains giving a large irreversible change in the magnetization. The TXM and PEEM observations revealed not only reversal via growth of domain chains in the columns (y) but also in the rows (x), which was reproduced by micromagnetic simulations that include a small angle between the applied field and the array columns. We established that the position of the chain ends is strongly influenced by the presence of the perpendicular chains during reversal, due to the ability to form a stable domain wall configuration when orthogonal chain ends meet and the formation of repulsive 360° walls which block the propagating chain boundaries when they approach a perpendicular domain, often resulting in the alignment of chain ends in rows. The resulting chain domain configuration is therefore highly dependent on the field history, i.e., the applied field strength and orientation. The switching field is mainly determined by domain nucleation and pinning of

chain ends. In addition, the higher fields required to annihilate the 360° walls result in small domains remaining towards the end of the reversal process.

The antidot arrays provide a model system for observation of nucleation, propagation, and pinning processes in a regular array of defects, made particularly easy to interpret by the discrete length of the domain chains. Our work provides an important insight into the mechanisms behind magnetization reversal and in particular, the possibility of controlling domain walls with well-defined magnetic configurations has implications for the design of future domain wall devices.[27] The switching fields are dominated by energy barriers related to the nucleation of domains, pinning of domain walls, and the annihilation of 360° walls. This information is particularly important with the advent of new lithography processes, which will allow future fabrication of much smaller antidot arrays.[28–31]

*Electronic address: laura.heyderman@psi.ch

†Also at Fachbereich Physik, Universität Konstanz, Universitätsstrasse 10, Konstanz, Germany.

‡Present address: School of Engineering, Computer Science and Mathematics, University of Exeter, EX4 4QF, United Kingdom.

[1] J. I. Martin, J. Nogues, K. Liu, J. L. Vicent, and I. K. Schuller, J. Magn. Magn. Mater. **256**, 449 (2003).

[2] B. D. Terris and T. Thomson, J. Phys. D **38**, R199 (2005).

[3] J. M. Daughton, A. V. Pohm, R. T. Fayfield, and C. H. Smith, J. Phys. D **32**, R169 (1999).

[4] M. M. Miller, G. A. Prinz, S. F. Cheng, and S. Bounnak, Appl. Phys. Lett. **81**, 2211 (2002).

[5] J. G. Zhu and Y. F. Zheng, in *Spin Dynamics in Confined Magnetic Structures I*, edited by B. Hillebrands and K. Ounadjela (Springer-Verlag, Berlin, 2002), Vol. 83, p. 289.

[6] C. T. Yu, H. Jiang, L. Shen, P. J. Flanders, and G. J. Mankey, J. Appl. Phys. **87**, 6322 (2000).

[7] A. O. Adeyeye, J. A. C. Bland, and C. Daboo, Appl. Phys. Lett. **70**, 3164 (1997).

[8] C. C. Wang, A. O. Adeyeye, and Y. H. Wu, J. Appl. Phys. **94**, 6644 (2003).

[9] J. M. Torres Bruna, J. Bartolomé, L. M. García Vinuesa, F. Garcia Sanchez, J. M. Gonzalez, and O. A. Chubykalo-Fesenko, J. Magn. Magn. Mater. **290**, 149 (2005).

[10] I. Guedes, M. Grimsditch, V. Metlushko, P. Vavassori, R. Camley,

B. Ilic, P. Neuzil, and R. Kumar, Phys. Rev. B **67**, 024428 (2003).

[11] P. Vavassori, G. Gubbiotti, G. Zangari, C. T. Yu, H. Yin, H. Jiang, and G. J. Mankey, J. Appl. Phys. **91**, 7992 (2002).

[12] C. T. Yu, M. J. Pechan, and G. J. Mankey, Appl. Phys. Lett. **83**, 3948 (2003).

[13] M. J. Pechan, C. T. Yu, R. L. Compton, J. P. Park, and P. A. Crowell, J. Appl. Phys. **97**, 10J903 (2005).

[14] C. T. Yu, M. J. Pechan, W. A. Burgei, and G. J. Mankey, J. Appl. Phys. **95**, 6648 (2004).

[15] S. McPhail, C. M. Gürtler, J. M. Shilton, N. J. Curson, and J. A. C. Bland, Phys. Rev. B **72**, 094414 (2005).

[16] L. J. Heyderman, F. Nolting, and C. Quitmann, Appl. Phys. Lett. **83**, 1797 (2003).

[17] L. J. Heyderman, H. H. Solak, F. Nolting, and C. Quitmann, J. Appl. Phys. **95**, 6651 (2004).

[18] A. Y. Toporov, R. M. Langford, and A. K. Petford-Long, Appl. Phys. Lett. **77**, 3063 (2000).

[19] L. Torres, L. Lopez-Diaz, O. Alejos, and J. Iniguez, J. Appl. Phys. **85**, 6208 (1999).

[20] L. Torres, L. Lopez-Diaz, and J. Iniguez, Appl. Phys. Lett. **73**, 3766 (1998).

[21] L. J. Heyderman, S. Czekaj, F. Nolting, E. Müller, P. Fischer, P. Gasser, and L. Lopez-Diaz, J. Appl. Phys. **99**, 063904 (2006).

[22] C. Quitmann, U. Flechsig, L. Patthey, T. Schmidt, G. Ingold,

M. Howells, M. Janousch, and R. Abela, Surf. Sci. **480**, 173 (2001).

[23] E. Bauer, J. Phys.: Condens. Matter **13**, 11391 (2001).

[24] A. Scholl, H. Ohldag, F. Nolting, J. Stohr, and H. A. Padmore, Rev. Sci. Instrum. **73**, 1362 (2002).

[25] P. Fischer, T. Eimüller, G. Schütz, M. Köhler, G. Bayreuther, G. Denbeaux, and D. Attwood, J. Appl. Phys. **89**, 7159 (2001).

[26] L. J. Heyderman, H. Niedoba, H. O. Gupta, and I. B. Puchalska, J. Magn. Magn. Mater. **96**, 125 (1991).

[27] D. A. Allwood, G. Xiong, C. C. Faulkner, D. Atkinson, D. Petit, and R. P. Cowburn, Science **309**, 1688 (2005).

[28] Z. L. Xiao, C. Y. Han, U. Welp, H. H. Wang, V. K. Vlasko-Vlasov, W. K. Kwok, D. J. Miller, J. M. Hiller, R. E. Cook, G. A. Willing, and G. W. Crabtree, Appl. Phys. Lett. **81**, 2869 (2002).

[29] F. J. Castano, K. Nielsch, C. A. Ross, J. W. A. Robinson, and R. Krishnan, Appl. Phys. Lett. **85**, 2872 (2004).

[30] A. Vovk, L. Malkinski, V. Golub, S. Whittenburg, C. O'Connor, J. S. Jung, and S. H. Min, J. Appl. Phys. **97**, 10J506 (2005).

[31] A. A. Zhukov, A. V. Goncharov, P. A. J. de Groot, P. N. Bartlett, and M. A. Ghanem, J. Appl. Phys. **93**, 7322 (2003).